Energy & Buildings 279 (2023) 112653

Contents lists available at ScienceDirect

Energy & Buildings

journal homepage: www.elsevier.com/locate/enb

Energy usage and human behavior modeling for residential bottom-up energy simulation

Nestor Pereira [a], Manel Martínez-Ramón [a]

[a] Department of Electrical and Computer Engineering, The University of New Mexico, 1, University of New Mexico, Albuquerque 87131-0001, NM, United States

ARTICLE INFO

Article history:
Received 20 August 2022
Revised 29 October 2022
Accepted 8 November 2022
Available online 21 November 2022

Keywords:
Load modeling
Occupancy
Simulation
Bottom-up
Energy consumption
Load profile
Residential sector
Behavior modeling
Time use survey
REMODECE

ABSTRACT

We introduce a probabilistic modeling for a disaggregated Bottom-up simulation of residential energy usage. Parametric probability distributions are modeled with parameters that have a natural explanation in terms of usage and appliance power. Human behavior such as sleep and home occupancy variables are considered too, with its corresponding trained probabilistic Models. Model parameters are adjusted by the minimization of the Kullback–Leibler divergence from known appliance and behavior usage data. Self-generated photovoltaic Energy is included in the simulation with a battery for storage and electric vehicle usage. Simulations match individual and aggregated usage load profiles in the European REMODECE and RSE Italian load data sets. Obtained Models are useful for residential disaggregated simulations allowing individual appliances to change from house to house. Probabilistic distributions can be used as prior knowledge for energy management systems, risk management, and grid failure prediction and can be adapted based on non-stationary real-time house behavior and appliance usage.

1. Introduction

In 2021 the U.S. Energy Information Administration estimated 60.8% of the U.S. electricity generation comes from fossil fuels and predicted a 21% increase in residential electricity by 2040 [1]. The U.S. electricity market is divided into three main electricity sectors: residential, commercial, and industrial, distributed almost equally [2]. The residential sector consists of about half of the peak demand, and can strongly affect electricity pricing, transmission, and minimal grid power requirements [3].

The residential sector is changing with the introduction of new technologies such as photovoltaic panels, space heaters, heat pumps, hybrid and electric vehicles. To integrate these fast-growing technologies on the generation and load side, improve the reliability of power distribution networks, implement demand-side management and gain knowledge of the changing load curve, detailed information on the new behavior of appliances, residential consumption, and individual solar generation is required.

1.1. State of the art

Power load forecasting has been an indispensable tool in the operation, control, and planning of the power grid over decades [4]. Residential power demand is strongly influenced by user behavior as mentioned in [5], therefore analyzing the user's presence in the house and sleep schedule can help us predict and disaggregate the demand using single individual appliances, which combined, can form the residential load profile.

Literature reports two different approaches to estimate residential loads as mentioned in [6]: Top-down and Bottom-up. The Top-down approach estimates load profiles of the residential sector based on measurements at mid voltage and low voltage level substations and national energy statistics. Then, energy consumption patterns are assigned to households according to their characteristics.

We focus on the Bottom-up approaches, since Top-down approaches won't allow disaggregating the residential load into its different appliances. This bottom-up approach builds load profiles of statistically representative households exploiting information on three different inputs: i) activities and behaviors of end users as shown in [7] where occupancy and sleep probability distributions are defined based on the individual user activities

https://doi.org/10.1016/j.enbuild.2022.112653
0378-7788/

obtained from the American Time User Survey (ATUS) dataset [8]. Also seen in article [9] where several occupancy profiles are defined based on the number and age of occupants and days of the week. ii) single appliance load consumption method used in [10], where time use data and census data combined with appliances load profiles are used for a complete house simulation. iii) In article [11] a set of appliances are mathematically defined and sampled, obtaining an entire house load simulation. A combination of inputs is used in article [12], where four different demographic clusters are defined (families, singles, couples and retired) and information from focus groups and surveys is used to obtain energy services use distributions to generate synthetic residential loads.

There is an ongoing transition from natural gas, wood, and other burning fuels to electric temperature-based appliances in an attempt to increase self-generated electricity usage and minimize non-renewable energy sources [13]. Air conditioning and heating, if electrical, can form a big part of the daily residential electricity consumption, therefore its modeling is crucial for a realistic and accurate modern house simulation.

Temperature house modeling following thermodynamic laws is a common solution to building a house temperature controller as described in [14] or just to obtain a thermal Model of the house, which can be later used as part of the house load modeling as shown in [15], where inside and outside temperature and wall temperature act as changing and measurable variables affected by indoors energy sources, such as heating, ventilation, and air conditioning controlled by the HVAC and outdoors heating sources such as solar radiance as shown in article [16].

Article [17] estimates the residential load profile of the future for the year 2040, where a high percentage of houses own an electric heat pump for residential temperature management and electric vehicles. Also, there is an increase in devices' electricity consumption and the inclusion of solar panel generation in most houses. This article presents 3 different scenarios, for different demand growth estimations. Scenario A is the base scenario where load demand growth comes from the integration of these new technologies. Scenario B also includes economic growth leading to a 1.5% load demand growth from the normal residential electricity demand. Scenario C assumes the integration of the new technologies but a decrease of 1% for the normal residential electricity demand.

1.2. Contribution

Rather than constructing prediction models, this paper is oriented to construct interdependent probabilistic distributions of the behavior of the household occupant, appliances, and electric vehicle combined with a non-probabilistic standard thermodynamic model for heating and cooling systems. These distributions are used for simulating and modeling an entire house, the parameters of these distributions for appliances are taken from REMODECE. Human behavior is obtained from the American Time Use Survey (ATUS) data set and electric vehicle mileage consumption comes from Ford's electrical vehicles empirical measurements found in article [18].

Unfortunately, there are no available data sets from the same population. While it can be assumed that the behaviors of different populations are similar, in the present work this assumption is not necessary for what we want to show is that interpretable parameters of the probabilistic distributions can be adjusted from these measurements and later be used in simulation and modeling. The parameters model appliance usage periods, appliance power, and similar, and they have real values. The aggregation of household simulations is very close to the measured curves.

Our simulated house includes solar generation from photovoltaic panels and an energy storage system. The appliance and electric vehicle probabilistic models are dependent on the resident's behavior models. In other words, for example, the probability of turning an appliance on when the house is not occupied is zero in all cases. If the house is occupied a 100%, the vehicle is not in use. For simplicity, in all simulations only one electrical vehicle per household is modeled, but the extension to several vehicles is straightforward.

The load demand profile obtained with our probability models using only REMODECE appliances is compared with the REMODECE data set load profile, and also with the RSE Italian data set load profile. A complete house simulation including all electrical appliances and systems possibly found in the modern house of the future is obtained by sampling all the probabilistic distributions. Since the addition of new technologies changes the load profile curve, we also compare this final simulation with the estimated load profile curves of the future found in article 19.

These adjusted Models can be combined with energy management systems, increasing their accuracy and decreasing their predictions' uncertainties. Models can learn from new house observations combining prior knowledge with new observations, and personalizing the system to the house appliances and residents' behaviors.

2. Methodology

2.1. Data

A combination of different data sets is used for modeling the appliance usage, human behavior, mileage consumption of the electric vehicle, and weather variables for temperature and solar radiance-related appliances and photovoltaic generation. Table 1 summarizes the data sets, their location, and purposes of use.

2.1.1. REMODECE

This data set comes from the European project REMODECE [19], whose objective was to contribute to the understanding of the energy consumption for different types of equipment, consumer behavior, and comfort levels and identify demand trends in a wide variety of houses from 12 different European countries. The data collection occurred from 2006 to 2008, analyzing existing studies, surveys, and metering campaigns, conducting household questionnaires done by expert interviewers, detail audits focusing on demand load profiles, and conducting own measurements for a series of residential appliances.

The results are averaged hourly load diagrams, that present the measured average power load P_M of each one of the appliances in a household, as shown in the examples of Fig. 1.

2.1.2. Human behavior data obtained from ATUS

American Time Use Survey [8] measures the fraction of time people spend doing various activities such as sleeping, working, child caring, and socializing. The data files include information from nearly 219,000 interviews conducted from 2003 to 2020. We are mostly interested in sleep data from 2013–2015.

Table 1
Data sets location and purpose.

Name project	Location	Purpose
REMODECE	Europe	Appliance probability usage
ATUS	USA	Sleep schedule and house presence
EV data	USA	EV mileage consumption
Weather	Albuquerque NM	Solar generation and HVAC scheduling

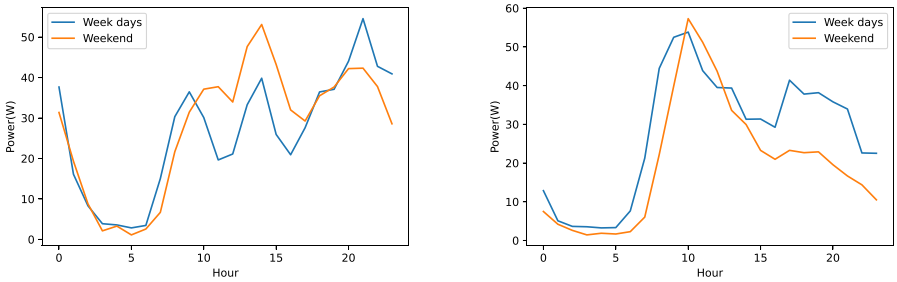

Fig. 1. Examples of REMODECE appliance hourly average power consumption. The left pane corresponds to the average hourly load of a dishwasher, while the right pane shows the average hourly load of a washing machine.

Presence profiles or occupancy data are obtained from article [7], which uses activities studied on the ATUS data categorized into "at home" or "away from home" to map to the presence or non-presence of occupants in the home differentiating between weekdays and weekends.

2.1.3. EV data

Our house has an electric vehicle that follows the mileage consumption behavior from data captured in article [18]. Data captured in Fig. 10 shows average miles per day for plug-in hybrid vehicles (PHEV) and battery electric vehicles (BEV).

2.1.4. PVGIS Solar radiation and weather database

This European solar generation database [20] has expanded and has data from the Americas and Africa. We used hourly solar radiance and weather parameters from Albuquerque, NM from 2013–2015. The measurements recorded in this database are:

- Power W
- Direct irradiance $\frac{W}{m^2}$
- Diffuse irradiance $\frac{W}{m^2}$
- Reflected irradiance $\frac{W}{m^2}$
- Total irradiance $\frac{W}{m^2}$
- Temperature (Celsius)
- Wind speed $\frac{m}{s}$

2.2. Probabilistic modeling of appliances and human behavior

For a given appliance, it is assumed that it may be used at different time instants resulting in different clusters defined with the letter j for different times of use. For example, from the REMODECE collected data, a washing machine can be modeled as an appliance used either in the morning or in the afternoon. A dishwasher is more likely to be used in the morning, afternoon, or evening, resulting in different clusters. The total energy consumption E of a given appliance can be modeled as:

$$P_M(t) = P \cdot P_u \sum_j p_j(on|t) P_j dt \tag{1}$$

where P is the nominal power of the appliance; P_u is the frequency of usage of the appliance, in other words, the probability that an appliance is used in a given day; $p_j(on|t)$ is the probability that the appliance is at ON state at instant t given that t belongs to cluster j and P_j is the posterior probability of cluster j, i.e. $P_j = p(j|on)$, or the probability of time belonging to cluster j provided that the machine is on.

The Model for the conditional probability $p_j(on|t)$ is, straightforwardly, the probability that instant t is higher than instant t_{on} when the appliance is switched on and lower than the instant t_{off} when the appliance is switched off. Therefore

$$\begin{aligned} p(on|t) &= p(t > t_{on}, t < t_{off}) = \\ &\int_t^{T_f} \int_0^t p(t_{on}) p(t_{off}|t_{on}) dt_{on} dt_{off} \end{aligned} \tag{2}$$

In this expression, $p(t_{on})$ represents the probability density of switching on at instant t_{on}, and $p(t_{off}|t_{on})$is the probability density of switching off at instant t_{off}, which is, in general, dependent on the switch on time instant. T_f represents the time length of a day.

The goal of this modeling is to find parametric Models for these two probabilities, whose parameters are explanatory of the usage of the appliances or the human behavior inside the household. These parameters can be adjusted by finding analytic expressions for $p(on|t)$ and adjusting them to match the observed usage graphs presented in SubSection 2.1. The criterion to be used for the optimization is the minimization of the Kullback–Leibler divergence between the theoretical expression (1) and each one of the empirical graphs. The adjustment must include not only the parameters of each one of the conditional probabilities but also the posteriors p_j, while the nominal power P of the appliance and the frequency of usage p_u are assumed to be known.

2.3. Appliance and user behavior models

This section presents the Models for the common appliances and the human behavior of a household. These Models are represented through probability distributions of the observed events, for example, turning on and off a device or leaving the house and returning.

2.3.1. Sigmoid-sigmoid probability model

This Model is proposed for those behaviors that can be modeled as a binary variable that changes its state at a given time and then it changes back to the previous one at a later time but where both events can be approximated as independent. For example, the occupancy of the house is "1" in the morning up to a given instant, where it switches to "0". In the afternoon or evening, the house starts being occupied again (the state switches to "1" again). It is assumed in this Model that these instants are independent. Therefore, the state probability with respect to time can be expressed with a product of probabilities as $p(on|t) = p(t > t_{on}, t < t_{off}) = P(t > t_{on}) \cdot P(t < t_{off})$. Therefore, the Model can be written as:

$$\begin{aligned} p(on|t) &= P(t > t_{on}) \cdot P(t < t_{off}) = \\ &\int_t^{T_f} p(t_{on|t}) dt_{on} \cdot \int_0^t p(t_{off|t}) dt_{off} \end{aligned} \tag{3}$$

Suitable cumulative probability density functions $P(t > t_{on}), P(t < t_{off})$are sigmoid functions with slope parameters γ_1 and γ_2 and mean parameters μ_1 and μ_2 and with approximate expressions:

$$P(t > t_{on}) = \int_t^{T_f} p(t_{on}) dt_{on} \approx \frac{1}{1 + e^{\gamma_1 (\mu_1 - t)}} \tag{4}$$

$$P(t < t_{off}) = \int_0^t p(t_{off})dt_{off} \approx \frac{1}{1 + e^{\gamma_2(t-\mu_2)}} \tag{5}$$

In order to use this approximations, we assume that $p(0 > t_{on}) = \frac{1}{1+e^{\gamma_1\mu_1}} \approx 0$ and $p(T_f > t_{on}) = \frac{1}{1+e^{\gamma_1(\mu_1-T_f)}} \approx 1$, and similarly for the PMF $p(t < t_{off})$. This approximation is valid if γ_1 and γ_2 are sufficiently large. The Model is then written as

$$p(on|t) \quad = \frac{1}{1+e^{\gamma_1(\mu_1-t)}} \cdot \frac{1}{1+e^{\gamma_2(t-\mu_2)}} \tag{6}$$

2.3.2. Gaussian-uniform probability model

A Gaussian-Uniform probability Model is suitable for those appliances modeled as having a probability density of switching on around a mean, that can be approximately represented by a Gaussian distribution, and where the probability of switching off is distributed between a minimum and a maximum value and that can be approximately represented by a uniform distribution $\mathcal{U}(\cdot)$ with width T_2 between $T_1 + t_{on}$ and $T_1 + t_{on} + T_2$. The distributions are, respectively:

$$\begin{aligned} p(t_{on}) \quad &= \frac{1}{\sigma\sqrt{2\pi}} e^{-\frac{(t_{on}-\mu)^2}{2\sigma^2}} \\ p(t_{off}|t_{on}) \quad &= \mathcal{U}_{[T_1+t_{on}, T_1+t_{on}+T_2]}(t_{off}) \end{aligned} \tag{7}$$

The Gaussian assumes that the instant when the appliance is connected has a mean μ and a variance σ^2. We make the approximation that, for suitable values of the mean and the variance, the Gaussian is approximate by zero if $t_{on} \leqslant 0$. The uniform distribution assumes that the appliance will be disconnected at a time instant t_{off} distributed uniformly from $T_1 + t_{on}$ and $T_1 + T_{on} + T_2$.

By plugging Eq.(7) into Eq. (2) we see that the integral has to be solved separately for three cases, namely for $t \leqslant T_1$, for $T_1 \leqslant t \leqslant T_1 + T_2$, and $t \geqslant T_1 + T_2$, as follows:

Case1: $t \leqslant T_1$.

$$p(on|t) = \frac{1}{2}\text{erf}\left(\frac{t-\mu}{\sigma\sqrt{2}}\right) + \frac{1}{2}\text{erf}\left(\frac{\mu}{\sigma\sqrt{2}}\right) \tag{8}$$

Case2: $T_1 \leqslant t \leqslant T_1 + T_2$.

$$\begin{aligned} p(on|t) = \quad & \frac{\sigma\sqrt{2}}{2T_2\sqrt{\pi}} e^{-\frac{\mu^2}{2\sigma^2}} - \frac{\sigma\sqrt{2}}{2T_2\sqrt{\pi}} e^{-\frac{(t-T_1-\mu)^2}{2\sigma^2}} \\ & + \frac{1}{2}\text{erf}\left(\frac{t-\mu}{\sigma\sqrt{2}}\right) + \frac{T_1+T_2+\mu-t}{2T_2}\text{erf}\left(\frac{\mu}{\sigma\sqrt{2}}\right) \\ & - \frac{t-T_1-\mu}{2T_2}\text{erf}\left(\frac{t-T_1-\mu}{\sigma\sqrt{2}}\right) \end{aligned} \tag{9}$$

Case 3: $t \geqslant T_1 + T_2$.

$$\begin{aligned} & p(on|t) = \frac{t-T_1-T_2-\mu}{2T_2}\text{erf}\left(\frac{t-T_1-T_2-\mu}{\sigma\sqrt{2}}\right) \\ & - \frac{t-T_1-\mu}{2T_2}\text{erf}\left(\frac{t-T_1-\mu}{\sigma\sqrt{2}}\right) + \frac{1}{2}\text{erf}\left(\frac{t-\mu}{\sigma\sqrt{2}}\right) \\ & - \frac{\sigma\sqrt{2}}{2T_2\sqrt{\pi}} e^{-\frac{(t-T_1-\mu)^2}{2\sigma^2}} + \frac{\sigma\sqrt{2}}{2T_2\sqrt{\pi}} e^{-\frac{(t-T_1-T_2-\mu)^2}{2\sigma^2}} \end{aligned} \tag{10}$$

The complete derivation of these expressions can be found in the Appendix.

2.4. Parameter adjustment, Kullback–Leibler divergence

The Kullback–Leibler (KL) divergence measures the dissimilarity between two density distributions [21]. This divergence is also known as information divergence and relative entropy. If densities p and q exist with respect to a Lebesgue measure, the Kullback–Leibler divergence is given by:

$$\mathbb{KL}(p(x)|q(x)) = \int_{\mathbb{R}^d} p(x) \log\frac{p(x)}{q(x)}dx >= 0 \tag{11}$$

This divergence is finite whenever $p(x)$ is continuous with respect to $q(x)$ and it is only zero if $q(x) = p(x)$. To approximate the given parametric distributions to the empirical appliance loads and human behavior, we minimize the Lebesque measure between the distributions. We use a Nelder-Mead simplex algorithm [22] to obtain the optimal parameters.

2.4.1. Sigmoid-sigmoid probability Model parameters

The sigmoid-sigmoid probability Model represented in Eq. (6), used for occupancy and sleep human behaviors has 4 parameters to be optimized using KL divergence. Parameters μ_1 defines the mean and γ_1 is proportional to the *precision* of the first sigmoid. Namely, the variance of the distribution is $\sigma_1^2 = \pi^2/3\gamma_1^2$. This sigmoid models the waking up moment for sleep or leaving the house moment for occupancy. Parameters μ_2 and γ_2 define the same statistics for the second sigmoid, which models the going to bed moment for sleep or arriving back to the house moment for occupancy.

2.4.2. Gaussian-uniform parameters

The Gaussian-uniform Probability Model in Eqs. (8)–(10), is used for simulating appliances whose turning off time depends on its turning on time and its individual usage characteristics. Parameters μ and σ define the mean and standard deviation of the Gaussian used for modeling the turning-on time of the appliance. Parameters T_1 and T_2 are optimized and they define the time of the shortest interval and the time of the longest interval of usage of the specific appliance. These probabilities are multiplied by a C parameter which allows our probability distribution, which has a value between 0 and 1, to be adjusted to the original appliance power curve $P_M(t)$.

2.5. House thermodynamic modeling

A non-probabilistic dynamic modeling of the temperature behavior of the house based on known forecast weather variables allows us to simulate the electrical thermal appliance usage defined as a heat input Q_h. Similarly to article [16], heat input comes from the electrical consumption of the HVAC Q_{elec} and the temperature difference between the HVAC core temperature defined with sub-index h and the temperature of the indoor air defined with sub-index a divided by a thermal resistance R_h defining the efficiency of the heater. The higher the thermal resistance, the more heat it generates from electricity, therefore the higher the efficiency and vice versa. For this example, this resistance is considered very high, making the difference between temperatures insignificant and therefore converting all the electrical consumption into heat energy. The electrical consumption of the HVAC can be defined by how many watts are needed to change a degree of temperature to the HVAC core.

$$\begin{aligned} Q_h &= Q_{elec} - \frac{T_h - T_a}{R_h} \\ Q_{elec} &= C_h \frac{dT_h}{dt} \end{aligned} \tag{12}$$

Similarly to how the HVAC electrical consumption Q_{elec} affects the temperature of the HVAC, the heat input Q_h can affect the temperature of the air and therefore can be included in our thermodynamic Eq. 14

$$C_a \frac{dT_a}{dt} = Q_h \tag{13}$$

Human presence and equipment use can increase the indoor temperature. To avoid adding more degrees of complexity and since the main focus of the article is to find probabilistic parametric Models for appliance usage, these small temperature variations due to the occupancy and appliance heat dissipation are ignored.

Light heating is ignored since modern lighting, such as LEDs, is more efficient than old incandescent lamps, and has low power consumption and lower heat output. In article [14], thermodynamic equations are used for a Model-based predictive control of the house temperature, and house parameters defining house floor area, orientation, and physical properties are introduced. We use these equations and parameters for our non-probabilistic thermal modeling including solar irradiance.

$$\begin{aligned} &C_a \tfrac{dT_a}{dt} = C_a(T_a(t) - T_a(t-1)) = Q_h(t-1) \\ &-K_i(T_a(t-1) - T_w(t-1)) - K_f(T_a(t-1) - T_o(t-1)) \end{aligned} \tag{14}$$

$$\begin{aligned} &C_w \tfrac{dT_w}{dt} = C_w(T_w(t) - T_w(t-1)) = Q_s(t-1) \\ &+K_i(T_a(t-1) - T_w(t-1)) - K_o(T_w(t-1) - T_o(t-1)) \end{aligned} \tag{15}$$

where T_a is the indoor air temperature (C), T_w is the mean wall temperature (C), T_o is the outside air temperature (C); Q_h (kW) is the heat input to the air node. The Model uses five parameters: C_a (kJ/K) is the thermal capacity of the indoor air, C_w (kJ/K) represents the thermal capacitance of the wall, k_f (kW/K) is the conductance ascribed to ventilation and elements with little thermal capacitance, e.g. windows, K_i (kW/K) is the conductance between the indoor air and the wall, K_o (kW/K) is the conductance between the wall and the outside air, Q_s (kW) is the heat from the sun radiance.

To use the Model represented by Eqs. (14) and (15), these equations must be rewritten in a numerical form defining a sampling period T, expressed in seconds, and obtain our approximation:

$$\begin{aligned} &T_a(t) = T_a(t-1) + \\ &\tfrac{T\cdot(Q_h(t-1) - K_i(T_a(t-1) - T_w(t-1)) - K_f(T_a(t-1) - T_o(t-1)))}{C_a} \end{aligned} \tag{16}$$

$$\begin{aligned} &T_w(t) = T_w(t-1)) + \\ &\tfrac{T\cdot(Q_s(t-1) + K_i(T_a(t-1) - T_w(t-1)) - K_o(T_w(t-1) - T_o(t-1)))}{C_w} \end{aligned} \tag{17}$$

2.5.1. Parameter identification

In this subsection, we introduce a method to identify the physical parameters of the house avoiding the need of knowing the house area, materials, and orientation. Substituting Eq. 15 into 14 we can get an equation that depends only on T_a and T_o, which are known, and the unknown variable $T_w(t)$.

$$\begin{aligned} &\left(\tfrac{T(K_i+K_f)}{C_a} - 1 + \tfrac{T^2K_i^2}{C_a(C_w - TK_i - TK_o)}\right)T_a(t-1) \\ &+T_a(t) - \tfrac{T}{C_a}Q_h(t-1) + \left(\tfrac{T^2K_iK_o}{C_a(C_w + TK_i + TK_o)} - \tfrac{TK_f}{C_a}\right)T_c(t-1) \\ &+ \tfrac{T^2K_i}{C_a(C_w - TK_i - TK_o)}Q_s(t-1) \\ &= \tfrac{TK_i}{C_a}\tfrac{Cw}{Cw - TK_i - TK_o}T_w(t) \end{aligned} \tag{18}$$

We can use the same equation from (14) to obtain the next time instant $t+1$ equation.

$$\begin{aligned} C_a \tfrac{dT_a}{dt} = &\quad C_a(T_a(t+1) - T_a(t)) \\ = &\quad Q_h(t) - K_i(T_a(t) - T_w(t)) - K_f(T_a(t) - T_o(t)) \end{aligned} \tag{19}$$

Substituting $T_w(t)$ from 18 into 19, we get a final equation for time instants $t, t+1$ and $t-1$ that only depends on T_a, T_o, Q and Q_s at different time instants, which are known.

$$\begin{aligned} &T_a(t) - T_a(t+1) + \tfrac{T}{C_a}Q_h(t) + \left(\tfrac{T^2K_iK_o}{C_aC_w} - \tfrac{TK_f(C_w - TK_i - TK_o)}{C_aC_w}\right)T_o(t-1) \\ &- \tfrac{T(C_w - TK_i - TK_o)}{C_aC_w}Q_h(t-1) + \tfrac{C_w - TK_i - TK_o}{C_w}T_a(t) \\ &+ \left(\tfrac{T(C_w - TK_i - TK_o)(K_i+K_f)}{C_aC_w} - \tfrac{C_w - TK_i - TK_o}{C_w} + \tfrac{T^2K_i^2}{C_aC_w}\right)T_a(t-1) \\ &- \tfrac{TK_i}{C_a}T_a(t) - \tfrac{TK_f}{C_a}T_a(t) + \tfrac{TK_f}{C_a}T_o(t) + \tfrac{T^2K_i}{C_aC_w}Q_s(t-1) = 0 \end{aligned} \tag{20}$$

Using five equations like 20 for different time instants $t, t+1, t+2, t+3, t+4, t+5$ and known variables T_a, T_o, Q_h, Q_s for all those time instants, we can obtain the physical parameters C_a, C_w, K_i, K_f, K_o.

2.6. Electric vehicle consumption modeling

Looking at the EV data shown in Fig. 10, we can see that it follows a Gamma distribution. Using average mileage usage values and minimizing the KL divergence defining the dissimilarity between our gamma function and the original data, we can find the optimal parameters for the distribution that models the daily EV traveled distance.

$$x \sim p(k,\theta) = x^{k-1}e^{-\frac{x}{\theta}}\tfrac{1}{\Gamma(k)\theta^k} \tag{21}$$

where x is the distance, $k > 0$ is the shape parameter, $\theta > 0$ is the scale parameter and $\Gamma(\cdot)$ is the Gamma function.

2.7. Solar power generation modeling

In our PVGIS data set [20] we can see that solar irradiance and power generated simulated on the database are almost the same, therefore we can assume that solar irradiance captured by a pyranometer or solar device used for data capturing is almost the same as power generated by the photo-voltaic cell applying an efficiency factor of 15%.

3. Experiments

3.1. System architecture

Our experimental house consists of non-shiftable appliances, which form a base load, shift-able appliances, solar power generation with photovoltaic panels connected to a residential battery for extra energy storage, and an electric vehicle which usually charges in the evening/night with a level 2 EV charger.

3.1.1. Non shiftable appliances

These appliances are always on or turn on when the residents need them and cannot be changed because the comfort level of the resident would be strongly disrupted. The refrigerator and freezer are unshiftable constant appliances. AC, electric heater, lights, cooker, TVs, and a tank-less water heater, which heats water on-demand, turns on at different moments of the day, and shouldn't be shifted.

3.1.2. Shiftable and power regulated appliances

The washing machine, dishwasher, and dryer are time shiftable within a range defined by the user, this would give us flexibility and allow us to minimize peak demand and savings. The electric vehicle can be time-shifted and power regulated.

3.1.3. PV panels and battery

Solar generation decreases the amount of energy bought from the grid decreasing electricity cost and the use of grid non-renewable energy. We have a battery pack, which can store left-over generated electricity and use it whenever needed instead of buying it from the grid, decreasing costs, peak demand, and indirectly the effect on climate change.

3.2. Awake probability parameters

We use the probabilistic Models from Eq.(4) and (5) to model the probability of being awake obtained from the ATUS data (see 2.1.2), which, among other curves, shows the probability of that

the occupants are awake in residential buildings in the USA. The Probability Model is a combination of two sigmoid-sigmoid Models, one for the probability of awakening and another one for the probability of falling asleep. We separately calculate the wake-up time and bedtime of each individual in the house assuming they are independent of each other by minimizing the KL distance between the probabilistic Model and the data (see SubSection 2.4). Fig. 2 shows the original data and our sigmoid-sigmoid adjusted model.

Parameters μ_1 and μ_2 represent the average time residents wake up and go to bed. Parameters γ_1 and γ_2 express its variability respectively, where a higher γ represents less variability and smaller γ more variability, we could say that the Model's variance is inversely related to γ. Table 2 shows the optimized parameters The means μ_1 and μ_2 are expressed in hours and the values for γ_1 and γ_2 are expressed in hours^{-1}. C_1 and C_2 are adimensional.

We can see that the average time when people wake up is 6:22 AM and go to bed at 9:46 PM, going to bed has a smaller variability in time shown with a bigger γ and waking up has a higher variability in time shown with a slightly smaller γ.

This estimation gives an accurate Model according to the observed data. Nevertheless, the wake-up and sleep time estimates are not consistent with other published statistics. For example, Sleep cycle is a downloadable application for mobile devices which tracks sleeping behavior. In post [23], the app determines that the average American wakes up at 7:09 AM and goes to sleep at 11:39 PM. Sleep cycle data seems to be biased based on age and other characteristics, while ATUS data is a non-weighted nor biased average of different wake-up and going to bed times from Americans of all ages, work schedules, and characteristics. We also believe Sleep cycle data could be naturally biased given that many of its users are young adults and teenagers who are prone to the use of technological applications.

3.3. Occupancy probability parameters

We can use the same equations Eq. (4) and (5) to model the occupancy of the house, where the time of leaving the house and time of coming back are assumed independent from each other, just as done with awake probability. Weekdays have a higher total probability of leaving the house while on the weekends there is a smaller probability of leaving the house as shown in Fig. 3.

We can see the fitted Model parameters in Table 3. Means μ_1 and μ_2 represent the average time people leave the house and come back. Parameters γ represent the variability of the leaving time or coming back expressed in hours $^{-1}$. For weekdays and weekends, we can see a bigger variability in the time of coming back with a small γ and a smaller variability in the time of leaving the house with a bigger γ. Parameters C_1 and C_2 are mainly used to adjust the probability density to the original curve and are adimensional.

We end up finding out that on average, people leave their house at 7:09 AM and come back at 5:51 PM, which fits with our average waking up time and usual time when people leave their jobs.

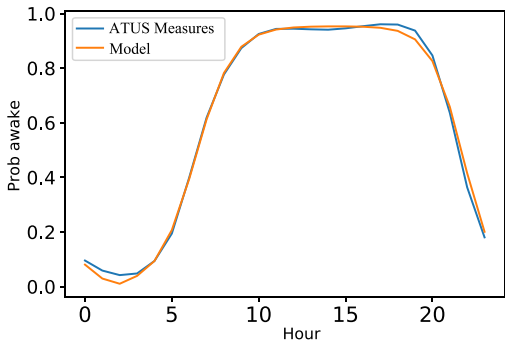

Fig. 2. Measured probability of being awake during weekdays as reported in [7] (in red), and adjusted probability Model. of being awake.

3.4. Appliance modeling

Using Eqs. ()()()(8)–(10)minimizing Kullback–Leibler divergence we can find the parameters that make our function fit the original data. These parameters also have a physical meaning of the appliance such as minimum cycle time as T_1, maximum cycle time as T_2, and nominal power P. Parameter C is directly related to the nominal power of the appliance times the probability of belonging to the specific cluster, times the frequency of usage of the appliance, as shown in the following equation, obtained from (1).

$$C_j = P \cdot P_u \cdot p_j(on|t) \tag{22}$$

When modeling appliances with Eqs. ()()()(8)–(10), parameters μ_i model the average time when appliances turn into on state, and σ_i model standard deviation of this time instant, for each different cluster i.

To find the optimal number of clusters, we compare the cost function values achieved with different numbers of clusters and find the number that minimizes the cost function without increasing too much the complexity of the total Model similar to the k-means clustering selection elbow method [24].

3.4.1. Dishwasher modeling

Using the appliance Model and parameter optimization explained above, we find that the dishwasher Model has 3 clusters, one for the morning, one after lunch, and one after dinner. A manually selected probability of daily usage P_u of 0.8, meaning it's used most of the days, and a nominal power of 790 W obtained from (22) after fitting the model.

In Fig. 4 we can see the fitting of the three clusters to the original data and the following Table 4 shows means and variance of the different clusters which match with breakfast, lunch, and dinner times. We can see that minimum cycles for the different clusters are values between 0.25 and 0.3 h and maximum cycles T_2 are between 1.38 and 1.58 h for the different clusters.

3.4.2. Washing machine modeling

For the case of the washing machine model, 2 clusters fit better the original data, a probability of daily usage P_u of 0.55 is chosen and a nominal power $P$of 1196 W is obtained after fitting.

Fig. 5 shows the morning cluster and the evening one, and we can see on Table 5 parameters defining means and variances of the different clusters. Also minimum and maximum cycles. Its minimum cycle goes between 0.25–0.29 h or around 15 min. T_2 maximum cycle for weekdays is 0.96 h and for the weekend is a longer cycle of 1.3 h.

3.4.3. Dryer modeling

The dryer Model has 3 clusters, a morning cycle from the previous day's washing machine's night cycle, a short midday cycle to dry the morning washing machine cycle, and a late night cycle after evening washing machine cycles. Manually chosen probability of daily usage P_u of 0.55 similar to the washing machine, gives us a nominal power $P$of 1749 W after fitting the Model depicted in Fig. 6.

Weekdays cycles are shorter, probably due to smaller loads, with a minimum cycle T_1 of 0.25–0.3 h and a maximum cycle T_2 of 1.58–1.67 with a short midday cycle of 0.25 to 0.8 h as depicted

Table 2
Parameters of the distributions of being awake

μ_1	γ_1	C_1	μ_2	γ_2	C_2
6.37	0.928	1	21.76	1.188	0.95

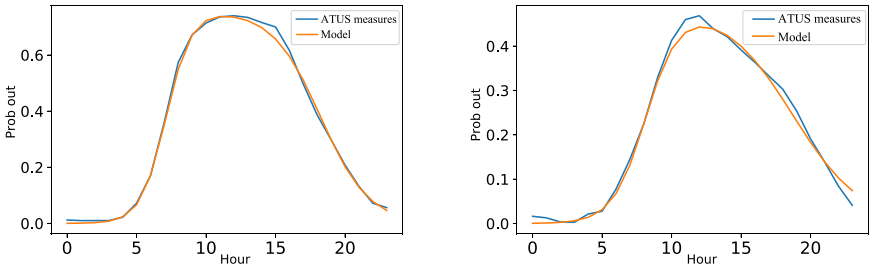

Fig. 3. Probability of being outside the house. Left pane: modeling probability of being away for weekdays. Right pane: modeling probability of being away for weekends.

Table 3
Parameters of the distributions of being outside the house for weekdays and weekends.

Week days					
μ_1	γ_1	C_1	μ_2	γ_2	C_2
7.15	1.088	0.94	17.9	0.64	0.96
Weekends					
μ_1	γ_1	C_1	μ_2	γ_2	C_2
7.17	0.784	0.88	19.37	0.48	0.69

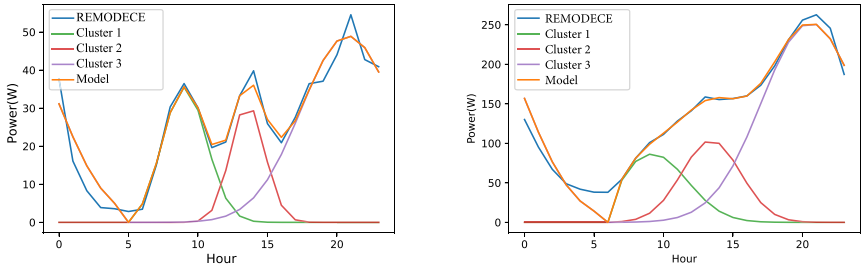

Fig. 4. Dishwasher usage modeling. Left pane: weekdays, right pane: weekend days.

Table 4
Dishwasher parameters for different clusters for week and weekends

Week days					
Cluster	μ	σ	T_1	T_2	C
1	8.22	1.47	0.25	1.44	124
2	13.29	1.09	0.27	1.38	174
3	20.50	3.34	0.26	1.49	353
Weekends					
Cluster	μ	σ	T_1	T_2	C
1	9.28	1.71	0.285	1.58	147
2	13.3	1.37	0.27	1.36	152
3	19.8	3.45	0.3	1.32	381

in Table 6. During weekends, minimum cycles increases to 0.35 h and maximum cycle T_2 can be as long as 2 h on late weekend days.

3.4.4. Cooker

The cooker Model has 3 clusters. Fig. 7 shows for weekdays, a morning and an evening cluster are predominant since few people have lunch at home and for the weekends, we can see a late breakfast and lunch cluster and a smaller but still important dinner cluster. It is assumed that the cooker is used more than once a day with a frequency of daily usage P_u of 1.6 and a nominal power $P$of 600 W is obtained.

Weekdays have a minimum cycle T_1 of 0.25 h and a longer morning maximum cycle T_2 of 2 h and an afternoon maximum cycle T_2 of 1.68 h. There is a midday cluster with a small C value, meaning a small probability of happening, with a very short cycle of around 0.3–0.34 which is around 20 min.

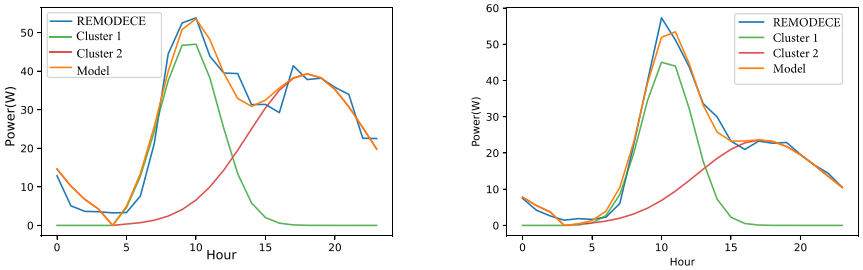

Fig. 5. Left pane: weekday, Right pane: weekend days.

Table 5
Parameters for washing machine for weekdays and weekends.

Week days					
Cluster	μ	σ	T_1	T_2	C
1	9.06	2.15	0.36	0.96	310
2	17.49	4.2	0.49	0.97	425
Weekends					
Cluster	μ	σ	T_1	T_2	C
1	9.8	1.81	0.48	1.25	193
2	16.51	4.55	0.57	1.31	219

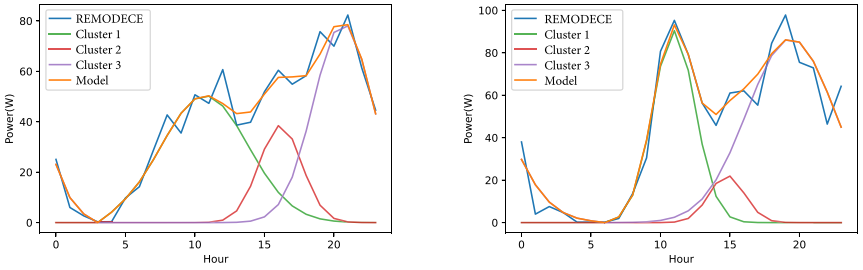

Fig. 6. Dryer data and Models for weekdays (left) and weekends.

Table 6
Parameters for dryer for weekdays and weekends

Week days					
Cluster	μ	σ	T_1	T_2	C
1	9.98	3	0.25	1.67	359
2	15.83	1.62	0.256	0.8	244
3	20	2.07	0.31	1.58	374
Weekends					
Cluster	μ	σ	T_1	T_2	C
1	10.33	1.44	0.34	1.54	309
2	14.21	1.20	0.37	1.30	69
3	18.60	3.10	0.35	2.00	508

On the weekends, the minimum cycle T_1 is 0.25 h, and the maximum cycle T_2 is 1.41–1.58 h. Results and parameters are shown in Fig. 7 and Table 7.

3.4.5. Water heater

For this appliance, we found that the optimal number of clusters varies between weekdays and weekends seen in Fig. 8. The water heater Model has 3 clusters on weekdays, the biggest one in the morning and then the other two are for the afternoon straight when people get home or late at night. During the weekend we only find 2 important clusters, one for the morning and another for the late afternoon since many activities happen on the weekend.

Water heaters are used more than once a day with a frequency of daily usage P_u of 1.7 and a nominal power $P$of 4500 W.

Weekday minimum cycle T_1 are similar around 0.25 h and morning and night maximum cycle T_2 are longer 1.45–1.75 h. Weekend days have a longer minimum cycle T_1 of 0.5–0.55 h and a shorter maximum cycle T_2 of 1.2–1.25 h. The values are summarized in Table 8.

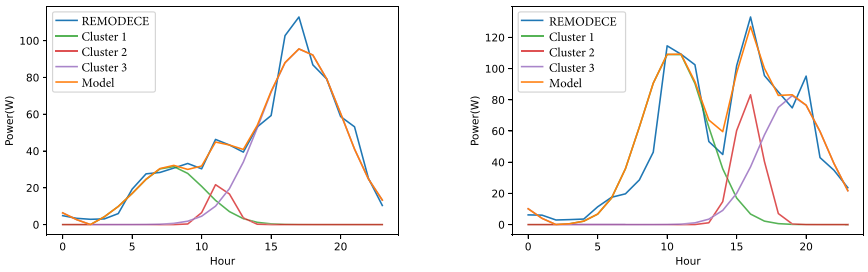

Fig. 7. Cooker.

Table 7
Parameters for the cooker for weekdays and weekends

Week days					
Cluster	μ	σ	T_1	T_2	C
1	7.42	2.89	0.25	2.02	187
2	11.09	0.65	0.30	0.34	70
3	16.65	2.80	0.25	1.68	631
Weekends					
Cluster	μ	σ	T_1	T_2	C
1	10.06	1.97	0.25	1.41	584
2	15.3	0.99	0.25	1.58	288
3	18.95	2.05	0.26	1.48	415

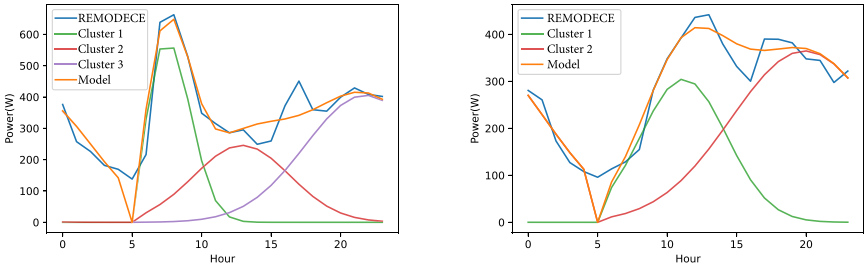

Fig. 8. Water heater.

Table 8
Parameters for the water heater for weekdays and weekends

Week days					
Cluster	μ	σ	T_1	T_2	C
1	6.85	1.53	0.27	1.75	1989
2	11.11	3.02	0.25	1.45	1432
3	20.25	5.1	0.27	1.68	4832
Weekends					
Cluster	μ	σ	T_1	T_2	C
1	10.71	3.14	0.5	1.2	2341
2	19.54	5.12	0.55	1.25	3896

3.4.6. Temperature based appliances

We simulate a house that has an electric heater of 7 kW of nominal power and air conditioning with a nominal power of 6 kW. The default temperature is set to 18 °C. We simulate temperature data for two consecutive days with Eq. (16) and (17) using initial parameters that represent the house physical behavior used in article [14] and a sampling rate (T) of 900 s (15 min) and results are shown in Fig. 9 for a winter day and a summer day.

We can obtain the previously manually selected physical parameters of the house using 5 different time instants from the temperature data and minimizing Eq. (20) for each time instant. We use the Basin-Hopping method [25] implemented in Python in the scipy.optimize package, with a step size of 10 and 200 iterations, to avoid local minimums and find a global minimum and the optimal parameters. Calculating the parameters 100 times for different days and time instants and averaging the results from all the iterations we estimate the parameter values in Table 9 including parameter value variation with its standard deviation.

We can see that the wall thermal capacity *Cw* has the highest variation, I believe this is caused because the solar radiance affects directly its temperature. Cloudy days don't see a strong change in wall temperature while sunny days do, making this variable change for different days.

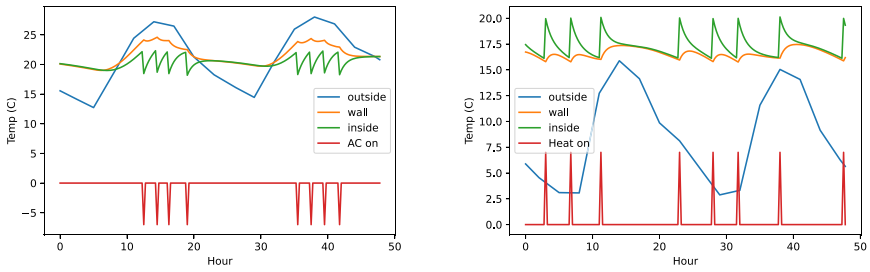

Fig. 9. Left pane: Cooling for a summer day, Right pane: Heating for a winter day.

Table 9
Parameters manually selected

Parameters	Ca	Cw	Ki	Kf	Ko
Original	1700	2100	0.35	0.035	0.02
Obtained	1711.7	2169	0.364	0.034	0.0228
σ	13.18	154.92	22.06	28.5	15.33

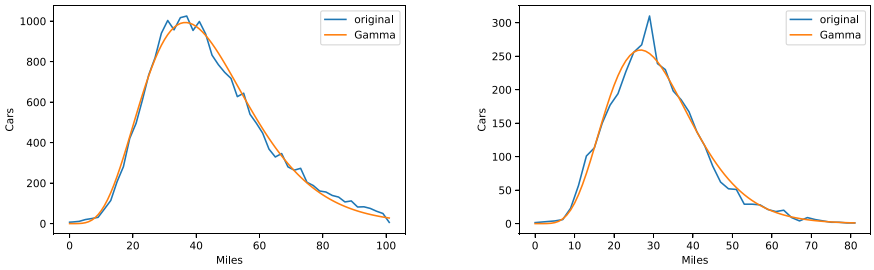

Fig. 10. Left: Gamma distribution for PHEV, Right: Gamma distribution for EV.

3.4.7. Electric vehicle

Most electric cars in the market get around 4 miles of autonomy for every kW of charge as mentioned in article [26]. The rated power of a level 2 Electric vehicle charger [26] is 7.4 kW at 230 V, where different levels of charging can be used.

Sampling the number of miles used during the day from our Gamma distributions adjusted to the original data from [18] and shown in Fig. 10 and knowing the charging rate we can obtain the power needed for a full charge. For our simulation, we'll assume the charge starts when the resident gets back home shown with the occupancy variable from Fig. 3.

3.4.8. House load profile

REMODECE load curve for a typical European household comes from its appliances' electricity consumption, excluding water heaters and space heaters and the use of electric vehicles. We obtained the weights P_u of the appliance's use from the REMODECE article [27] that studies the disaggregated electricity consumption. REMODECE monitors energy in 12 European countries including some colder countries such as Denmark or the Czech Republic, whose AC consumption is low. Considering that AC is only used during summer months, its daily probability of use for the entire year is low as shown in Table 10.

To test our probability Models combined accuracy, we can obtain a simulated daily load profile and compare it to other studies and data sets. To obtain our load profile, we run 1000 simulations for individual appliances with the probabilities of use from Table 10 and average their power consumption to obtain the resulting load profile. We ignore some low-power non-controllable or shiftable appliances included in the REMODECE data set since their impact on the load profile is small and can't be scheduled for energy savings purposes or electricity peak management. We compare our resulting load profile with daily load profiles from REMODECE data set [19] and RSE [28]. Article [10] uses a bottom-up approach based on Monte Carlo Non-Homogeneous Semi-Markov for appliance simulations combined with household end-user behaviors to simulate daily household load profiles. It compares its individual appliance simulations with REMODECE's hourly load diagrams and obtains an average daily load profile which it's also used as a benchmark. Most of the other bottom-up disaggregated simulation approaches lack some of the inputs considered in our article and are not directly comparable.

We can see in Fig. 11 that our simulation curve follows the same trend and has similar peak demand values as the other benchmark load profiles. Our curve differentiates slightly from the REMODECE load profile from the exclusion of the low power non-controllable or shiftable appliances and differentiates from the other data sets' load profiles due to different appliances' nominal power consumption rates and different daily probabilities of use. Table 11 shows 2 similarity metrics (MAPE, MRSE) between our simulation curve

Table 10
REMODECE appliance's P_u

Cooker	AC	Fridge	Lights	TV	Washing machine	dishwasher
0.75	0.045	0.9	7.6	0.35	0.75	0.7

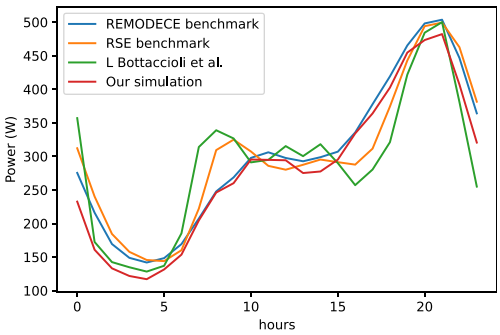

Fig. 11. Comparison of our house simulation with only REMODECE appliances load profile and the benchmark from different data sets including benchmark from Bottaccioli et al. [10].

Table 11
Caption.

Benchmark	MAPE	RMSE
REMODECE	7.789	24.429
RSE	12.17	41
Article [10]	13.86	54.33

and benchmark load profiles(REMODECE, RSE and article [10]), quantifying the visual difference mentioned previously. Just to clarify, these accuracy measures aren't as strict as needed for a prediction algorithm, since we are looking for simulations that follow a similar trend and maximum and minimum values frequently seen in typical house load profiles.

3.5. Simulation of a house in different scenarios

Before running a complete house simulation, the user needs to initialize parameters defining the house architecture and behavior such as the number of residents, area covered by solar panels (m^2), efficiency of the solar panels, battery capacity(kWh), type of car (electric/hybrid) and thermostat temperature set (°C).

Using Python's Pandas library to load calendar data for the dates of interest (2013–2015), we can classify days into week working days or weekends/holidays having different occupancy and appliance Models respectively. Hourly electricity prices used for calculating the total cost, come from the ISO NE Regional transmission Organization public database which can be found athttps://www.iso-ne.com.

Using the aforementioned data, we simulated in 15-min intervals individual appliances and their power consumption. The results can be seen in the top pane of Fig. 12. The bottom pane of the figure shows sleeping and occupancy indicators for a household with only one resident for a winter day. Human behavior such as wake-up time, sleep time, and time to leave the house and come back are shown. Sleep values of 1 mean that the resident is awake and occupancy values of 1 mean that the user is outside the house. The figure also shows times when residents are at home and awake with a variable named "available". At this time some appliances for example lights are turned on and limit the use of the rest appliances depending on human interaction. Some appliances such as washing machines and dishwashers only need human availability for the ON moment, while others like the cooker or the water heater require an awake person during the ON and the OFF moment. Most of the simulations will happen during times when residents are awake and in the house, ignoring the ones that happen outside the available period and re-simulating the appliance until the ON or OFF moment happens when residents are available. We introduce a limited number of re-simulations (N = 50), which is rarely needed, for rare availability cases such as very early morning wake up or late night sleeps where appliances have a low probability of usage.

House power consumption, sources, and battery data are shown in Fig. 13, where we can see how much electricity comes from the solar panels and how much is bought from the grid. The top left plot shows the total power production. A positive sign means that the produced power is higher than the used power, and hence the energy can be stored in the battery or the power can be injected into the grid. The top right plot shows the photovoltaic production of the house. The bottom left graph shows the energy stored in the battery and the power signal measured by the battery. A positive power value corresponds to a charging process, thus the slope of the battery energy is positive. The battery energy reaches a maximum value in this example at around 2 pm. The bottom right pane shows the grid power behavior. A negative value indicates that the grid is injecting power into the house, and a positive value means that the house is selling the leftover power (that is not used or that cannot be stored in the battery) to the grid.

We can see on the lower right plot of Fig. 13 that grid energy is used in the early morning for cold days to heat up the house with the electric heating system and the solar power generation covers part of the afternoon load and even sells some extra energy that can't be stored, to the grid shown as a positive power in the power grid graph.

Figs. 14 and 15 show the simulation of a house with 2 residents and different occupancy schedules, therefore different appliance

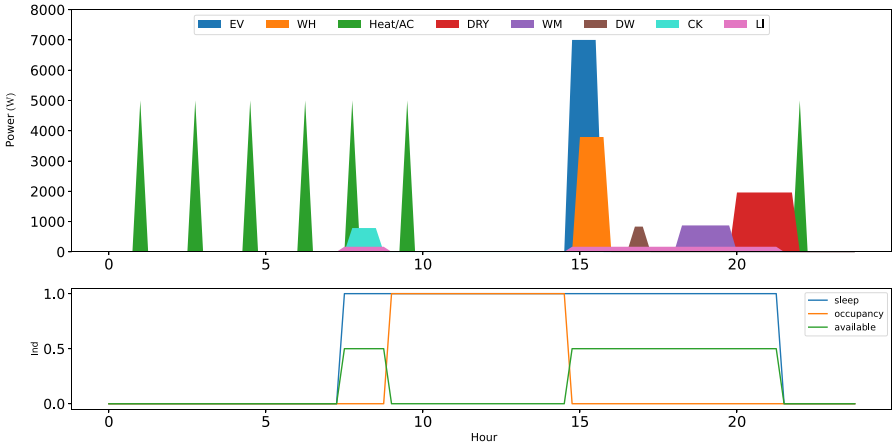

Fig. 12. Appliances profiles and human behavior.

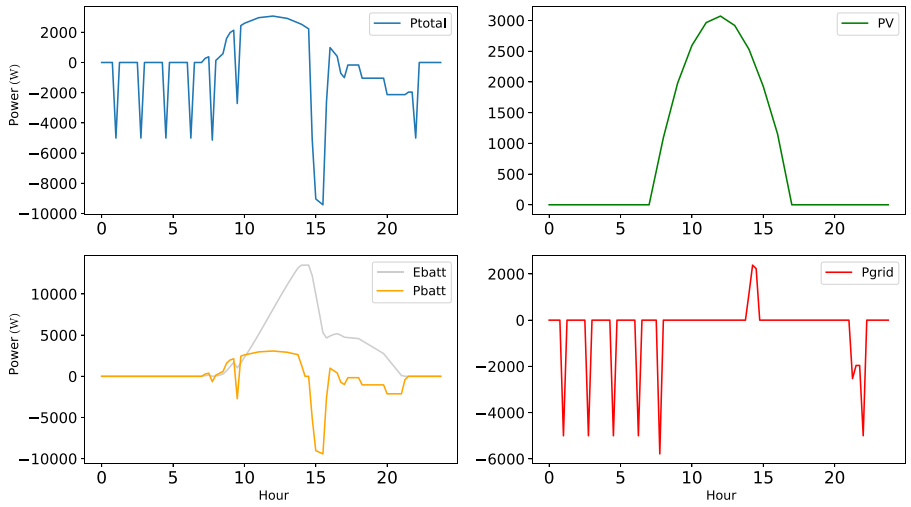

Fig. 13. Power usage.

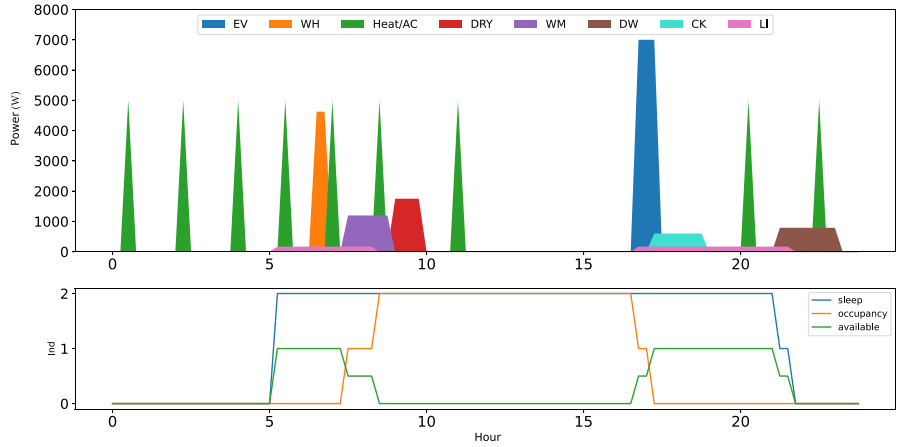

Fig. 14. Profiles of usage of an experiment similar to one of Figs. 12 and 13, with the difference that in this house the number of occupants is changed to 2.

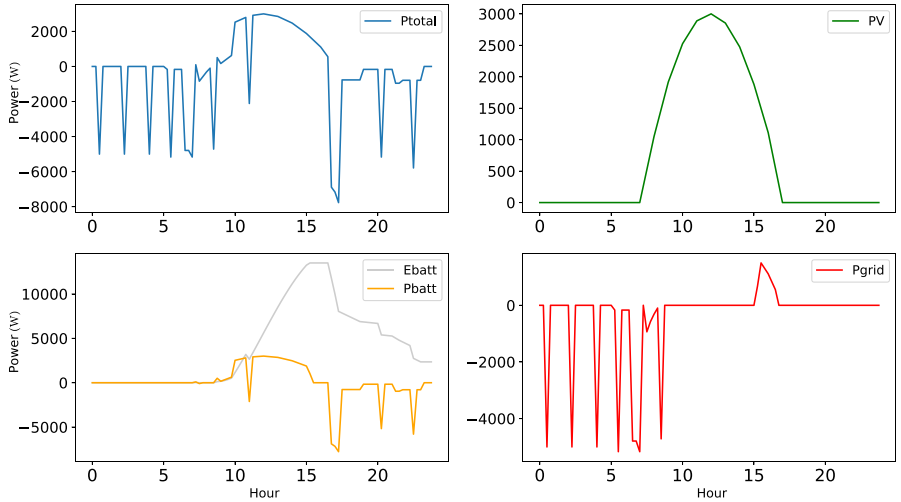

Fig. 15. Power usage for the experiment shown in Fig. 15. As can be seen, in this particular example, the battery is fully charged for about two hours and there is power left f. or the next day.

usage. We can see in this simulation how the battery is not fully discharged by the end of the day and it has some energy left for the next day.

In Fig. 16 and 17 we find a house simulation with 3 residents for a summer day when air conditioning is used mainly during daylight hours. For this specific hot day, solar power generation covers

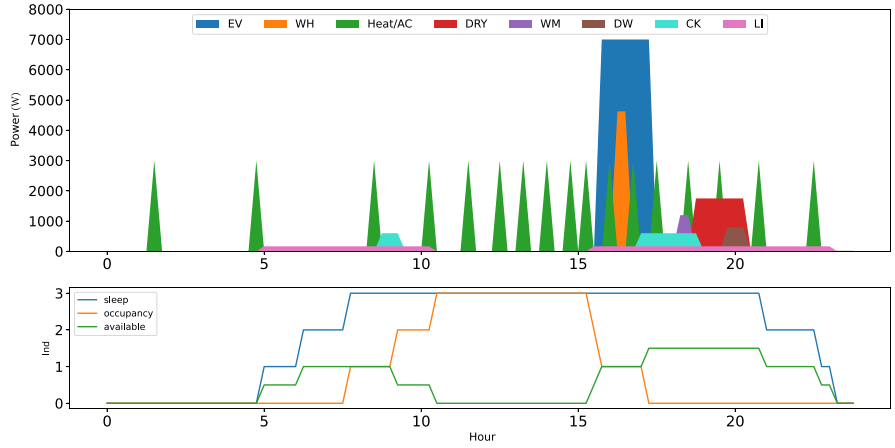

Fig. 16. Appliances profiles and human behavior on a simulation with three users in a summer scenario.

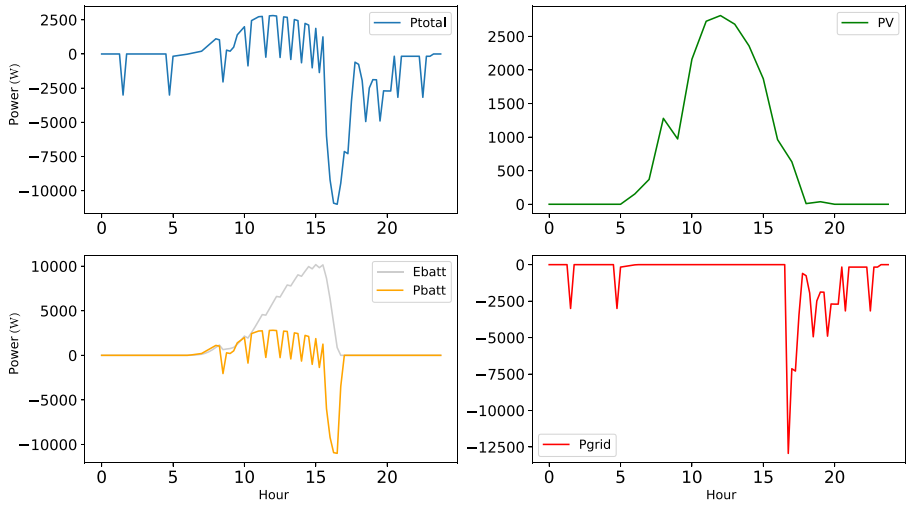

Fig. 17. Power usage for the simulation of Fig. 16.

almost all the house AC power consumption but the charging of the electric vehicle later afternoon drains the battery making the system buy grid electricity and leaving it with no more energy for the next day.

In the above simulations, the daily frequency of usage of all appliances is the same through all the scenarios in spite of the number of occupants. Indeed, the usage of most appliances is independent of the number of household members present in the house. For example, washing machines will be used the same number of times a week with a low dependency on the number of users, but in the case of a low number of users, the clothes loads will be simply lower. A similar situation is encountered in the case of TV or stove usage.

4. Discussion

The simulations in SubSection 3.4 show an accurate modeling of the behavior of appliances and household members, and a reasonable interpretation of the parameters of the probabilistic Models in terms of the appliance and human behavior and a simulation of a household with the same appliance usage frequency produces results very similar to the ones measured in the REMODECE and RSE benchmarks.

Nevertheless, the simulated households presented in SubSection 3.5 will not produce profiles similar to the ones in REMODECE and RSE. The reason for this is that many old houses use gas for space and water heating and the PV generation and EV usage are not significant in the aggregated loads. These kinds of scenarios were simulated in Fig. 11. In particular, EVs are big electricity consumers, and they usually consume most of the afternoon battery's energy leaving it depleted and having to buy electricity from the grid for upcoming house appliance usage.

In the Fig. 18 we compare the benchmark profile load curves with our simulated house load curve. Our simulated house uses electrical space and water heaters, electrical air conditioning, and electric vehicles both running on the grid or solar electricity generation affecting and changing the total daily load demand curve for the next upcoming years, which could leave old load profiling methods obsolete. Indeed, running our house Model with all the electrical appliances mentioned shows a new different load profile curve. Increasing the total electricity consumption from the single household's typical daily consumption of 7.2 kWh to 32 kWh.

In the article, [17] future residential demand load curves for 2040 are estimated. This future residence includes electricity-powered heat pumps, Photovoltaic generation, and electric vehicles. 3 future scenarios are presented in this article. Scenario A is the average scenario where demand growth in normal residential

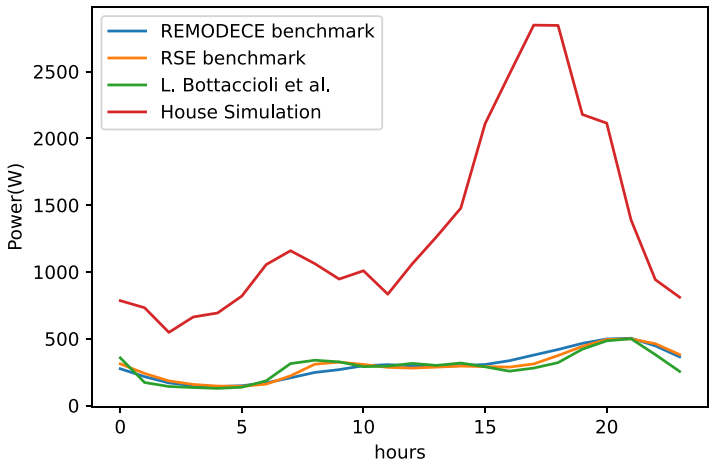

Fig. 18. Comparison of benchmark house load profile with the simulated load profile generated from hour house with all electrical appliances.

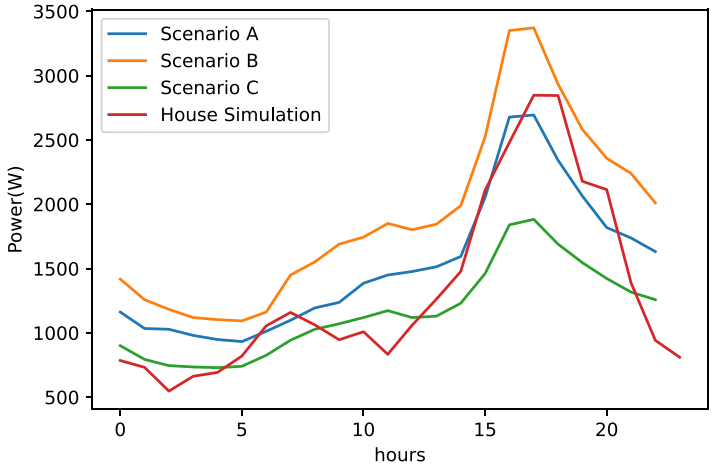

Fig. 19. Comparison of our house simulation load profile with the future load profiles estimated for 3 different scenarios in article [17]. The difference between scenarios is explained in the pre.vious paragraph.

electricity use is 0%, 40% of vehicles are electric and 50% of houses use heat pumps. Scenario B considers an increase in electricity demand and assumes 75% of vehicles are electric and 80% of houses use heat pumps. Scenario C considers a decrease in normal residential electricity, but still considers a high percentage of electric vehicles and heat pumps (75%). In Fig. 19 we compare our simulated load curve with the load profiles estimated in the article mentioned for all three different scenarios. Due to the lack of articles, modeling appliance usage and simulating load profiles for houses including EV, PV, and electric thermal appliances, we compare our simulation results with the previous article which gives us a futuristic load profile with different data sources and methodology, therefore curves are not expected to exactly match. With that said, we can see that our simulated load profile follows the residential future curve estimations closely, proving our simulation methodology with probability distributions including the appliances soon seen in modern houses.

5. Conclusion

The obtained results assume that electricity consumption is going to increase dramatically in the upcoming years, supporting The Energy Information Administration (EIA) estimation of a 40% increase in residential electrical usage by 2040. Energy management systems could be the solution to distributing energy consumption during the day and lowering our electricity costs. modeling morning electricity consumption, buying low-cost/low-demand night electricity, and storing it in the battery could substantially reduce electricity costs caused by morning heating systems and lower the morning peak demand. For this purpose, this work presents a comprehensive methodology to model individual home appliances, human behavior, temperature-regulating appliances (AC and space heating), and electric vehicle consumption for a complete house simulation. All Models but the temperature-regulating appliances are probabilistic. Thermal appliances are based on a physical Model which follows thermodynamic equations and use indoor and outdoor temperature values to control the desired temperature.

The appliance Models and the human behavior Models are adjusted to the statistical data sets found in the REMODECE and ATUS repositories through the use of a KL divergence criterion and a gradient descent algorithm.

The appliance Models are constructed by using a combination of a Gaussian distribution for modeling the turning on instant and a uniform distribution which limits its shortest running cycle and its maximum cycle. This distribution, named Gaussian-uniform throughout the paper, is quite complex in its derivation and formulation, but it has been demonstrated to be an accurate approximation when adjusted to the REMODECE data set. The

parameters of the distribution are interpretable and their values are reasonable.

The human behavior Models are constructed with the use of sigmoidal functions that model the cumulative density distributions of being home and being out of the house. We model the probability of sleeping similarly. The parameters of the derived distributions are also interpretable. These parameters are adjusted from the ATUS data.

The EV Models for the usage in terms of daily driven distance are found to fit a Gamma function adequately when adjusted to data obtained from article [18] for electric and hybrid vehicles.

The presented results show that running a simulation using the obtained trained Models with only the REMODECE appliances results in a load profile matching accurately the load profile curve from the REMODECE data set and similar to the RSE data set. Our individual appliance simulations fit more accurately the original REMODECE appliance curves than in article [10].

Individual 15-min interval house simulations with different scenarios are shown and analyzed showing the benefits of including PV generation and battery in our system and the big impact on energy consumption that electric vehicles bring.

A final house load profile including all appliances, electric space and water heater, power generation systems, and electric vehicles is compared to the REMODECE, RSE, and article [10] and later on to article [17] curves showing how the transition from fossil fuel sources to electric systems and vehicles is going to change the typical household load profile in the upcoming years.

Future work includes the usage of the presented Models in decision-making methods for household energy management. Indeed, the generated appliance Models give us prior information on appliance usage and can be combined with adaptive optimization algorithms for energy management systems to improve their performance through the intrinsic capabilities of these probabilistic and physical Models to estimate uncertainty.

These Models could become adaptive by combining prior knowledge with changes obtained from new observations, thus making the energy management systems a smart real-time learner and fully personalized for each house and residents. This may be useful to estimate the likelihood of the events observed in a household or a community, which makes these Models useful in tasks related to fault or cyber-attack detection.

Data availability

Data will be made available on request.

Declaration of Competing Interest

The authors declare that they have no known competing financial interests or personal relationships that could have appeared to influence the work reported in this paper.

Acknowledgments

This work is partially supported by the grants EPSCoR OIA-1757207 (NSF, USA) and the King Felipe VI Endowed Chair of the UNM.

Authors would like to thank UNM Center for Advanced Research Computing, supported in part by the NSF, for providing high-performance computing, large-scale storage, and visualization resources.

Appendix A. Appendix

The mathematical path to obtaining our probability Model used for modeling the appliances is shown below. There is an integration process that divides the solution into three different cases based on the values of t, therefore three different equations. The derivations are computed by using the equality

$$\begin{aligned} p(on|t) &= p(t > t_{on}, t < t_{off}) = \\ &\int_t^{T_f} \int_0^t p(t_{on}) p(t_{off}|t_{on}) dt_{on} dt_{off} \end{aligned}$$

where the distributions are respectively

$$\begin{aligned} p(t_{on}) &= \frac{1}{\sigma\sqrt{2\pi}} e^{-\frac{(t_{on}-\mu)^2}{2\sigma^2}} \\ p(t_{off}|t_{on}) &= \mathcal{U}_{[T_1+t_{on}, T_1+t_{on}+T_2]}(t_{off}) \end{aligned} \tag{23}$$

The following cases are considered.

A.1. Case 1: $t < T_1$

In this case, as illustrated in Fig. 20 the product of both functions is nonzero for $T_1 \leqslant t_{off} \leqslant T_1 + T_2 + t$, as depicted by the striped area in the figure. This integral can be decomposed into three integrals corresponding to the left triangle, the central square, and the right triangle that form the stripe rhomboid of the figure. Therefore, the computation is decomposed into the three following integrals. The first one is the triangle between 0 and t in the t_{on} axis and between T_1 and $T_1 + t$ in the t_{off}n axis.

$$\begin{aligned} &\frac{1}{T_2} \int_{T_1}^{T_1+t} \int_0^{t_{off}-T_1} \frac{1}{\sigma\sqrt{2\pi}} e^{-\frac{(t_{on}-\mu)^2}{2\sigma^2}} dt_{on} dt_{off} = \\ &= \frac{t-\mu}{2T_2} \operatorname{erf}\left(\frac{t-\mu}{\sigma\sqrt{2}}\right) + \frac{\sigma\sqrt{2}}{2T_2\sqrt{\pi}} e^{-\frac{t^2-2\mu t+\mu^2}{2\sigma^2}} + \frac{t-\mu}{2T_2} \operatorname{erf}\left(\frac{\mu}{\sigma\sqrt{2}}\right) - \frac{\sigma\sqrt{2}}{2T_2\sqrt{\pi}} e^{-\frac{\mu^2}{2\sigma^2}} \end{aligned} \tag{24}$$

whose solution is a linear combination of error functions $\operatorname{erf}(\cdot)$ and square exponentials. The second one is the rectangle between $t_{off} = T_1 + t$ and $t_{off} = T_1 + T_2$

$$\frac{1}{T_2} \int_{T_1+t}^{T_1+T_2} \int_0^t \frac{1}{\sigma\sqrt{2\pi}} e^{-\frac{(t_{on}-\mu)^2}{2\sigma^2}} dt_{on} dt_{off} = \frac{T_2-t}{2T_2} \operatorname{erf}\left(\frac{t-\mu}{\sigma\sqrt{2}}\right) + \frac{T_2-t}{2T_2} \operatorname{erf}\left(\frac{\mu}{\sigma\sqrt{2}}\right) \tag{25}$$

which has a similar solution. Finally, the triangle in $T_1 + T_2 \leqslant t_{off} \leqslant T_1 + T_2 + t$ is integrated.

$$\begin{aligned} &\frac{1}{T_2} \int_{T_1+T_2}^{T_1+T_2+t} \int_{t_{off}-T_1-T_2}^{t} \frac{1}{\sigma\sqrt{2\pi}} e^{-\frac{(t_{on}-\mu)^2}{2\sigma^2}} dt_{on} dt_{off} = \\ &= \frac{\mu}{2T_2} \operatorname{erf}\left(\frac{t-\mu}{\sigma\sqrt{2}}\right) - \frac{\sigma\sqrt{2}}{2T_2\sqrt{\pi}} e^{-\frac{t^2-2\mu t+\mu^2}{2\sigma^2}} + \frac{\mu}{2T_2} \operatorname{erf}\left(\frac{\mu}{\sigma\sqrt{2}}\right) + \frac{\sigma\sqrt{2}}{2T_2\sqrt{\pi}} e^{-\frac{\mu^2}{2\sigma^2}} \end{aligned} \tag{26}$$

Adding everything together, the probability can be expressed as:

$$p(on|t) = \frac{1}{2} \operatorname{erf}\left(\frac{t-\mu}{\sigma\sqrt{2}}\right) + \frac{1}{2} \operatorname{erf}\left(\frac{\mu}{\sigma\sqrt{2}}\right) \tag{27}$$

A.2. Case 2: $T_1 < t < T_1 + T_2$

In case 2, the values of t seem to affect the mathematical solution of the double integrals creating two new subcases.

A.2.1. Case 2A: $t < T_2$

This situation is depicted in Fig. 21. We break the integral into three intervals. The first one is for $T_1 \leqslant t_{off} \leqslant T_1 + t$.

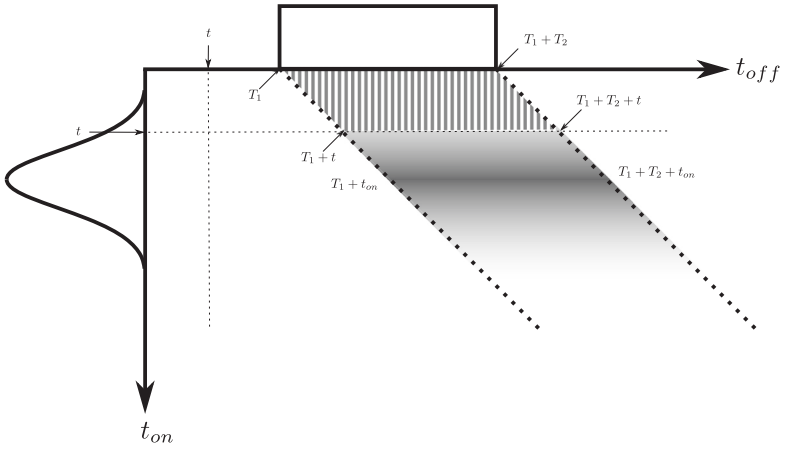

Fig. 20. Graphical illustration of the integral intervals for the computation of the probability distributions for Case 1, where $t \leqslant T_1$. The horizontal line corresponds to the domain of t_{off}, and the dotted line represents,$p(t_{off}|t_{on}])$, this is, the probability of t_{off}, which is dependent on t_{on}. The gray area corresponds to the intersection of the Gaussian function modeling $p(t_{on})$ with the pulse modeling $p(t_{off}|t_{on})$. Variable t_{on} is integrated between 0 and t and t_{off} is integrated between t and ∞. The area to be integrated is the striped one.

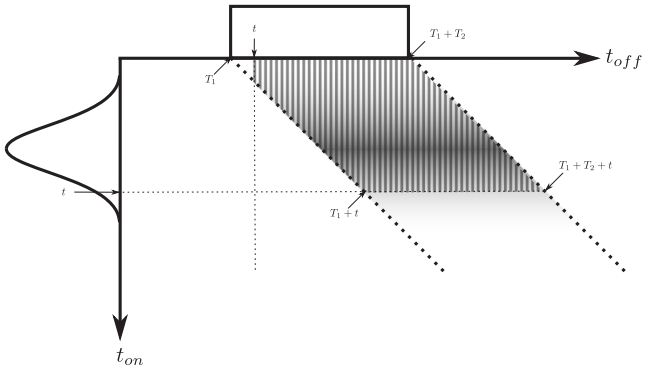

Fig. 21. Area of integration of the case 2A, where $T_1 \leqslant t \leqslant T_1+T_2$ and $t \leqslant T_2$, where T_2 is the length of the rectangle representing the uniform pdf.

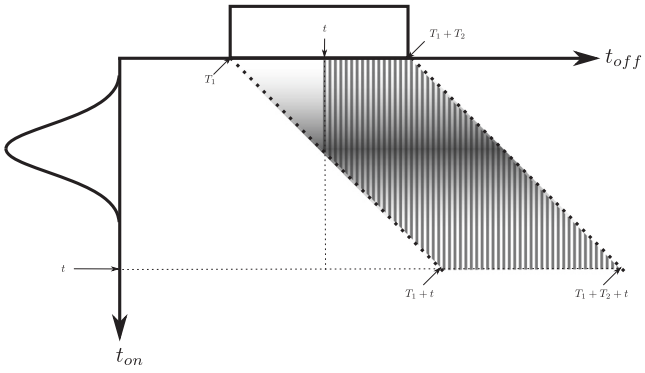

Fig. 22. Area of integration of the case 2B, where $T_1 \leqslant t \leqslant T_1+T_2$ and $t \geqslant T_2$.

$$\begin{aligned}&\frac{1}{T_2}\int_t^{T_1+t}\int_0^{t_{off}-T_1}\frac{1}{\sigma\sqrt{2\pi}}e^{-\frac{(t_{on}-\mu)^2}{2\sigma^2}}dt_{on}dt_{off}\\&=\frac{t-\mu}{2T_2}\mathrm{erf}\left(\frac{t-\mu}{\sigma\sqrt{2}}\right)+\frac{\sigma\sqrt{2}}{2T_2\sqrt{\pi}}e^{-\frac{t^2-2\mu t+\mu^2}{2\sigma^2}}\\&-\frac{t-T_1-\mu}{2T_2}\mathrm{erf}\left(\frac{t-T_1-\mu}{\sigma\sqrt{2}}\right)-\frac{\sigma\sqrt{2}}{2T_2\sqrt{\pi}}e^{-\frac{(t-T_1-\mu)^2}{2\sigma^2}}+\frac{T_1}{2T_2}\mathrm{erf}\left(\frac{\mu}{\sigma\sqrt{2}}\right)\end{aligned}\tag{28}$$

The second one is $T_1+t \leqslant t_{off} \leqslant T_1+T_2$.

$$\begin{aligned}&\frac{1}{T_2}\int_{T_1+t}^{T_1+T_2}\int_0^{t}\frac{1}{\sigma\sqrt{2\pi}}e^{-\frac{(t_{on}-\mu)^2}{2\sigma^2}}dt_{on}dt_{off}=\\&=\frac{T_2-t}{2T_2}\mathrm{erf}\left(\frac{t-\mu}{\sigma\sqrt{2}}\right)+\frac{T_2-t}{2T_2}\mathrm{erf}\left(\frac{\mu}{\sigma\sqrt{2}}\right)\end{aligned}\tag{29}$$

The third one is $T_1+T_2 \leqslant t_{off} \leqslant T_1+T_2$.

$$\begin{aligned}&\frac{1}{T_2}\int_{T_1+T_2}^{T_1+T_2+t}\int_{t_{off}-T_1-T_2}^{t}\frac{1}{\sigma\sqrt{2\pi}}e^{-\frac{(t_{on}-\mu)^2}{2\sigma^2}}dt_{on}dt_{off}=\\&=\frac{\mu}{2T_2}\mathrm{erf}\left(\frac{t-\mu}{\sigma\sqrt{2}}\right)-\frac{\sigma\sqrt{2}}{2T_2\sqrt{\pi}}e^{-\frac{t^2-2\mu t+\mu^2}{2\sigma^2}}+\frac{\mu}{2T_2}\mathrm{erf}\left(\frac{\mu}{\sigma\sqrt{2}}\right)+\frac{\sigma\sqrt{2}}{2T_2\sqrt{\pi}}e^{-\frac{\mu^2}{2\sigma^2}}\end{aligned}\tag{30}$$

A.2.2. Case 2B: $t > T_1+T_2$

Fig. 22 shows the case where $t > T_2$, which modifies the way in which the area must be divided for its integration. The first one is now $t \leqslant t_{off} \leqslant T_1+T_2$, the second one is $T_1+T_2 \leqslant t_{off} \leqslant T_1+t$, and the third one is $T_1+T_2 \leqslant t_{off} \leqslant T_1+T_2+t$. The solutions of the three integrals are the following.

$$\begin{aligned}&\frac{1}{T_2}\int_t^{T_1+T_2}\int_0^{t_{off}-T_1}\frac{1}{\sigma\sqrt{2\pi}}e^{-\frac{(t_{on}-\mu)^2}{2\sigma^2}}dt_{on}dt_{off}=\\&=\frac{T_2-\mu}{2T_2}\mathrm{erf}\left(\frac{T_2-\mu}{\sigma\sqrt{2}}\right)+\frac{\sigma\sqrt{2}}{2T_2\sqrt{\pi}}e^{-\frac{(T_2-\mu)^2}{2\sigma^2}}\\&-\frac{t-T_1-\mu}{2T_2}\mathrm{erf}\left(\frac{t-T_1-\mu}{\sigma\sqrt{2}}\right)-\frac{\sigma\sqrt{2}}{2T_2\sqrt{\pi}}e^{-\frac{(t-T_1-\mu)^2}{2\sigma^2}}+\frac{T_1+T_2-t}{2T_2}\mathrm{erf}\left(\frac{\mu}{\sigma\sqrt{2}}\right)\end{aligned}\tag{31}$$

$$\begin{aligned}&\frac{1}{T_2}\int_{T_1+T_2}^{T_1+t}\int_{t_{off}-T_1-T_2}^{t}\frac{1}{\sigma\sqrt{2\pi}}e^{-\frac{(t_{on}-\mu)^2}{2\sigma^2}}dt_{on}dt_{off}=\\&=\frac{\mu}{2T_2}\mathrm{erf}\left(\frac{t-\mu}{\sigma\sqrt{2}}\right)-\frac{\sigma\sqrt{2}}{2T_2\sqrt{\pi}}e^{-\frac{t^2-2\mu t+\mu^2}{2\sigma^2}}\\&+\frac{\mu}{2T_2}\mathrm{erf}\left(\frac{\mu}{\sigma\sqrt{2}}\right)+\frac{\sigma\sqrt{2}}{2T_2\sqrt{\pi}}e^{-\frac{\mu^2}{2\sigma^2}}\end{aligned}\tag{32}$$

$$\begin{aligned}&\frac{1}{T_2}\int_{T_1+t}^{T_1+T_2+t}\int_{t_{off}-T_1}^{t}\frac{1}{\sigma\sqrt{2\pi}}e^{-\frac{(t_{on}-\mu)^2}{2\sigma^2}}dt_{on}dt_{off}=\\&=\frac{\mu-T_2}{2T_2}\mathrm{erf}\left(\frac{t-\mu}{\sigma\sqrt{2}}\right)-\frac{\sigma\sqrt{2}}{2T_2\sqrt{\pi}}e^{-\frac{t^2-2\mu t+\mu^2}{2\sigma^2}}\\&+\frac{T_2-\mu}{2T_2}\mathrm{erf}\left(\frac{T_2-\mu}{\sigma\sqrt{2}}\right)+\frac{\sigma\sqrt{2}}{2T_2\sqrt{\pi}}e^{-\frac{(T_2-\mu)^2}{2\sigma^2}}\end{aligned}\tag{33}$$

The solution of this case is found by adding the six previous integrals:

$$\begin{aligned}p(on|t)=\;&\frac{1}{2}\mathrm{erf}\left(\frac{t-\mu}{\sigma\sqrt{2}}\right)+\frac{T_1+T_2+\mu-t}{2T_2}\mathrm{erf}\left(\frac{\mu}{\sigma\sqrt{2}}\right)+\frac{\sigma\sqrt{2}}{2T_2\sqrt{\pi}}e^{-\frac{\mu^2}{2\sigma^2}}\\&-\frac{\sigma\sqrt{2}}{2T_2\sqrt{\pi}}e^{-\frac{(t-T_1-\mu)^2}{2\sigma^2}}-\frac{t-T_1-\mu}{2T_2}\mathrm{erf}\left(\frac{t-T_1-\mu}{\sigma\sqrt{2}}\right)\end{aligned}\tag{34}$$

A.3. Case 3: $t > T_1 + T_2$

The third case is solved similarly but in this case the limits for t_{off} are simply between t and $t_1 + T_2 + t$, and the result is

$$\begin{aligned}&\frac{1}{T_2}\int_t^{t+T_1+T_2}\int_{t_{off}-T_1-T_2}^{t}\frac{1}{\sigma\sqrt{2\pi}}e^{-\frac{(t_{on}-\mu)^2}{2\sigma^2}}dt_{on}dt_{off}=\\&=\frac{T_1+T_2+\mu-t}{2T_2}\mathrm{erf}\left(\frac{t-\mu}{\sigma\sqrt{2}}\right)-\frac{\sigma\sqrt{2}}{2T_2\sqrt{\pi}}e^{-\frac{t^2-2\mu t+\mu^2}{2\sigma^2}}\\&+\frac{t-T_1-T_2-\mu}{2T_2}\mathrm{erf}\left(\frac{t-T_1-T_2-\mu}{\sigma\sqrt{2}}\right)+\frac{\sigma\sqrt{2}}{2T_2\sqrt{\pi}}e^{-\frac{(t-T_1-T_2-\mu)^2}{2\sigma^2}}\end{aligned}\tag{35}$$

$$\begin{aligned}&\int_t^{t+T_1}\frac{1}{T_2}dt_{off}\int_{t_{off}-T_1}^{t}\frac{1}{\sigma\sqrt{2\pi}}e^{-\frac{(t_{on}-\mu)^2}{2\sigma^2}}dt_{on}=\\&=\frac{T_1-t+\mu}{2T_2}\mathrm{erf}\left(\frac{t-\mu}{\sigma\sqrt{2}}\right)-\frac{\sigma\sqrt{2}}{2T_2\sqrt{\pi}}e^{-\frac{t^2-2\mu t+\mu^2}{2\sigma^2}}\\&+\frac{t-T_1-\mu}{2T_2}\mathrm{erf}\left(\frac{t-T_1-\mu}{\sigma\sqrt{2}}\right)+\frac{\sigma\sqrt{2}}{2T_2\sqrt{\pi}}e^{-\frac{(t-T_1-\mu)^2}{2\sigma^2}}\end{aligned}\tag{36}$$

Adding all terms, the result is

$$\begin{aligned}p(on|t)=\;&\frac{t-T_1-T_2-\mu}{2T_2}\mathrm{erf}\left(\frac{t-T_1-T_2-\mu}{\sigma\sqrt{2}}\right)\\&-\frac{t-T_1-\mu}{2T_2}\mathrm{erf}\left(\frac{t-T_1-\mu}{\sigma\sqrt{2}}\right)+\frac{1}{2}\mathrm{erf}\left(\frac{t-\mu}{\sigma\sqrt{2}}\right)\\&-\frac{\sigma\sqrt{2}}{2T_2\sqrt{\pi}}e^{-\frac{(t-T_1-\mu)^2}{2\sigma^2}}+\frac{\sigma\sqrt{2}}{2T_2\sqrt{\pi}}e^{-\frac{(t-T_1-T_2-\mu)^2}{2\sigma^2}}\end{aligned}\tag{37}$$

References

[1] [Online]. Available: URL: https://www.eia.gov/tools/faqs/faq.php?id=427&t=3.
[2] [Online]. Available: URL: https://www.epa.gov/energy/electricity-customers.
[3] [Online]. Available: URL: https://www.eia.gov/todayinenergy/detail.php?id=42915.
[4] Ó.G. Hinde, V.G. Verdejo, M. Martínez-Ramón, Forecast-informed power load profiling: A novel approach, Eng. Appl. Artif. Intell. 96 (2020).
[5] A.J. Collin, G. Tsagarakis, A.E. Kiprakis, S. McLaughlin, Development of low-voltage load models for the residential load sector, IEEE Trans. Power Syst. 29 (5) (2014) 2180–2188.
[6] A. Grandjean, J. Adnot, G. Binet, A review and an analysis of the residential electric load curve models, Renew. Sustain. Energy Rev. 16 (9) (2012) 6539–6565.
[7] D. Mitra, Y. Chu, K. Cetin, Cluster analysis of occupancy schedules in residential buildings in the United States, Energy Build. 236 (2021).
[8] American time use survey (ATUS). [Online]. Available: URL: https://www.bls.gov/tus/home.htm.
[9] D. Mitra, N. Steinmetz, Y. Chu, K.S. Cetin, Typical occupancy profiles and behaviors in residential buildings in the United States, Energy Build. 210 (2020).
[10] L. Bottaccioli, S. Di Cataldo, A. Acquaviva, E. Patti, Realistic multi-scale modeling of household electricity behaviors, IEEE Access 7 (2018) 2467–2489.
[11] M. Nijhuis, M. Gibescu, J. Cobben, Bottom-up Markov Chain Monte Carlo approach for scenario based residential load modelling with publicly available data, Energy Build. 112 (2016) 121–129.
[12] A. Mammoli, M. Robinson, V. Ayon, M. Martínez-Ramón, C.-F. Chen, J.M. Abreu, A behavior-centered framework for real-time control and load-shedding using aggregated residential energy resources in distribution microgrids, Energy Build. 198 (2019) 275–290.
[13] J.M. Cansino, M. d. P. Pablo-Romero, R. Román, and R. Yñiguez, Promoting renewable energy sources for heating and cooling in EU-27 countries, Energy Policy, 39(6), pp. 3803–3812, 2011.
[14] R. Bălan, J. Cooper, K.-M. Chao, S. Stan, R. Donca, Parameter identification and model based predictive control of temperature inside a house, Energy Build. 43 (2–3) (2011) 748–758.
[15] K.P. Schneider, J.C. Fuller, Detailed end use load modeling for distribution system analysis, IEEE PES General Meeting, IEEE (2010) 1–7.
[16] P. Fazenda, P. Lima, P. Carreira, Context-based thermodynamic modeling of buildings spaces, Energy Build. 124 (2016) 164–177.
[17] E. Veldman, M. Gibescu, H.J. Slootweg, W.L. Kling, Scenario-based modelling of future residential electricity demands and assessing their impact on distribution grids, Energy Policy 56 (2013) 233–247.
[18] D. Boston, A. Werthman, Plug-in vehicle behaviors: An analysis of charging and driving behavior of ford plug-in electric vehicles in the real world, World Electric Vehicle J. 8 (4) (2016) 926–935.
[19] A. De Almeida, P. Fonseca, B. Schlomann, N. Feilberg, and C. Ferreira, "Residential monitoring to decrease energy use and carbon emissions in Europe," in International Energy Efficiency in Domestic Appliances & Lighting Conference, 2006.
[20] Photovoltaic geographical information system. [Online]. Available: URL: https://re.jrc.ec.europa.eu/pvg_tools/en/#HR.
[21] F. Perez-Cruz, "Kullback-Leibler divergence estimation of continuous distributions," 2008 IEEE Int. Symposium on Information Theory, pp. 1666–1670, 2008.
[22] Nelder-mead scipy, optimize documentation. [Online]. Available: URL: https://docs.scipy.org/doc/scipy/reference/optimize.minimize-neldermead.html.
[23] Sleepcycle app sleeping data. [Online]. Available: URL: https://www.sleepcycle.com/sleep-science/what-we-know-about-americas-healthiest-happiest-best-rested/.
[24] M. Cui, Introduction to the k-means clustering algorithm based on the elbow method, Acc., Audit. Finance 1 (1) (2020) 5–8.
[25] D.J. Wales, J.P. Doye, Global optimization by basin-hopping and the lowest energy structures of Lennard-Jones clusters containing up to 110 atoms, J. Phys. Chem. A 101 (28) (1997) 5111–5116.
[26] G.R.C. Mouli, P. Venugopal, and P. Bauer, "Future of electric vehicle charging," 2017 International Symposium on Power Electronics (Ee), pp. 1–7, 2017.
[27] A. De Almeida, P. Fonseca, B. Schlomann, N. Feilberg, Characterization of the household electricity consumption in the EU, potential energy savings and specific policy recommendations, Energy Build. 43 (8) (2011) 1884–1894.
[28] S. Maggiore, "Evaluation of the effects of a tariff change on the Italian residential customers subject to a mandatory time-of-use tariff," ECEEE 2013 SUMMER STUDY, 2013.